BioMACROMOLECULES

Article

pubs.acs.org/Biomac

Conformational Conversion during Controlled Oligomerization into Nonamylogenic Protein Nanoparticles

Julieta M. Sánchez,[†,‡] Laura Sánchez-García,[§,∥] Mireia Pesarrodona,[†,§,∥,▽] Naroa Serna,[†,§,∥] Alejandro Sánchez-Chardi,[⊥] Ugutz Unzueta,[†,§,∥,#] Ramón Mangues,[∥,#] Esther Vázquez,[*,†,§,∥] and Antonio Villaverde[*,†,§,∥]

[†]Institut de Biotecnologia i de Biomedicina, Universitat Autònoma de Barcelona, Bellaterra 08193 Barcelona, Spain

[‡]Universidad Nacional de Córdoba, Facultad de Ciencias Exactas, Físicas y Naturales, ICTA and Departamento de Química, Cátedra de Química Biológica, Córdoba, Argentina, CONICET, Instituto de Investigaciones Biológicas y Tecnológicas (IIBYT), Córdoba, Argentina, Av. Velez Sarsfield 1611, X5016GCA Córdoba, Argentina

[§]Departament de Genètica i de Microbiologia, Universitat Autònoma de Barcelona, Bellaterra, 08193 Barcelona, Spain

[∥]CIBER de Bioingeniería, Biomateriales y Nanomedicina (CIBER-BBN), Bellaterra, 08193 Barcelona, Spain

[⊥]Servei de Microscòpia, Universitat Autònoma de Barcelona, Bellaterra, 08193 Barcelona, Spain

[#]Biomedical Research Institute Sant Pau (IIB-Sant Pau) and Josep Carreras Research Institute, Hospital de la Santa Creu i Sant Pau, 08025 Barcelona, Spain

ABSTRACT: Protein materials are rapidly gaining interest in materials sciences and nanomedicine because of their intrinsic biocompatibility and full biodegradability. The controlled construction of supramolecular entities relies on the controlled oligomerization of individual polypeptides, achievable through different strategies. Because of the potential toxicity of amyloids, those based on alternative molecular organizations are particularly appealing, but the structural bases on nonamylogenic oligomerization remain poorly studied. We have applied spectrofluorimetry and spectropolarimetry to identify the conformational conversion during the oligomerization of His-tagged cationic stretches into regular nanoparticles ranging around 11 nm, useful for tumor-targeted drug delivery. We demonstrate that the novel conformation acquired by the proteins, as building blocks of these supramolecular assemblies, shows different extents of compactness and results in a beta structure enrichment that enhances their structural stability. The conformational profiling presented here offers clear clues for understanding and tailoring the process of nanoparticle formation through the use of cationic and histidine rich stretches in the context of protein materials usable in advanced nanomedical strategies.

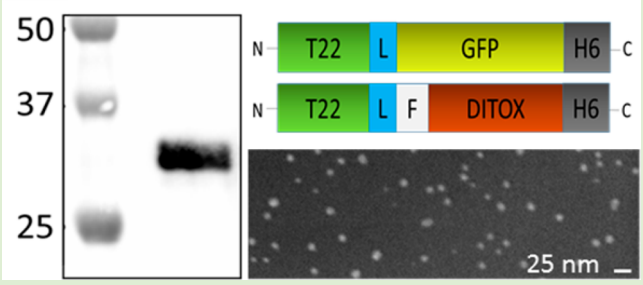

INTRODUCTION

Protein materials are gaining interest in materials sciences and in nanomedicine because of the intrinsic biocompatibility and nonrecalcitrant nature of polypeptides that makes their use in drug delivery or regenerative medicine safer than other micro- or nanoscale composites.[1] Additionally, biologically and environmentally friendly fabrication of proteins in recombinant organisms[2] and the possibility to modulate their structure and function through genetic engineering[3] allow the generation of tailored functional or multifunctional materials,[4] with unique characteristics such as a plasticity unreachable by metals, polymers, ceramics, or other nanostructured materials. The construction of protein-based materials relies on the controlled oligomerization of individual polypeptides, which act as building blocks of complex supramolecular arrangements. This is achieved by the engineering of natural oligomerization domains, by domain-swapping, or through the regulation of protein−protein contacts by a diversity of strategies,[1b,2b] among which one of the best exploited is controlled amyloid fibril formation.[1a,5] The structural conversion from isolated protein monomers to components of larger amyloidal structures has been studied and reviewed in detail,[6] and the analysis of the conformational changes along the process allows designing new categories of building blocks for novel tailored materials[7] with potentially improved properties and functionalities.[1a,6a,8]

Among nonfibril protein materials, isometric nanoparticles (NPs) resulting from protein self-assembling are of special interest in cell-targeted delivery of protein and nonprotein drugs.[9] In this context, cationic protein segments such as polyarginines, as short peptides[10] or as N-terminal protein fusions,[11] promote self-assembling.[12] Supported by this

Received: June 13, 2018
Revised: July 23, 2018
Published: July 27, 2018

DOI: 10.1021/acs.biomac.8b00924
Biomacromolecules XXXX, XXX, XXX−XXX

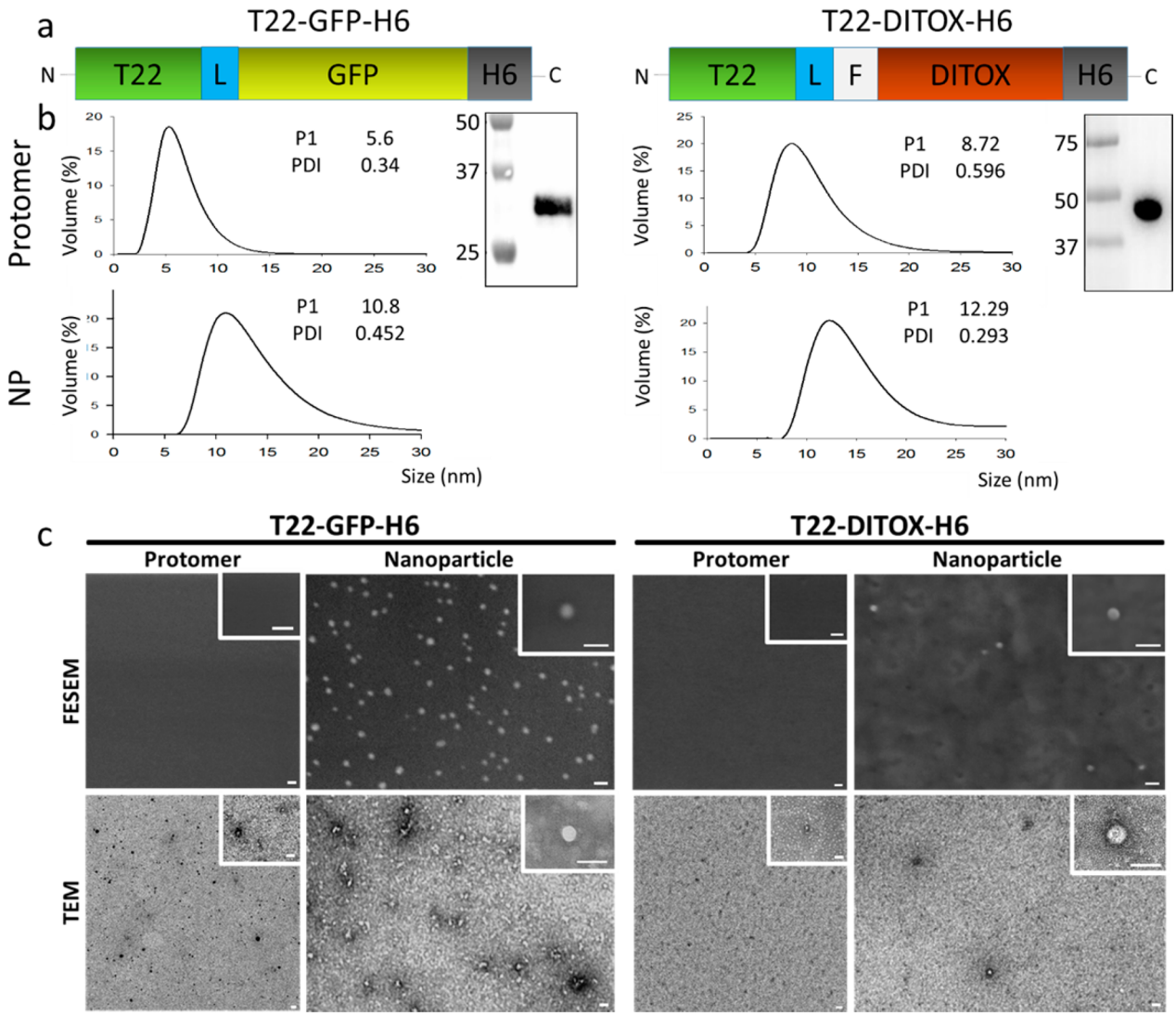

Figure 1. (a) Modular organization of T22-GFP-H6 and T22-DITOX-H6. L corresponds to a peptidic linker that confers molecular flexibility, and F corresponds to a furin cleavage site. Box sizes are only indicative. Additional details of the constructions are given elsewhere.[19a,22] (b) DLS measurements of disassembled (top) and assembled (bottom) proteins. Numbers indicate mean peak size and polydispersion index (PDI), in nanometers. In the inset, Western blot analyses of purified proteins. Numbers indicate the molecular mass or markers (in kDa). (c) FESEM and TEM of protomers and NPs. Bar size is 25 nm.

principle, T22-GFP-H6 and related fusion proteins are fluorescent building blocks that self-assemble as cyclic homomeric NPs of 10−20 nm[11] through the combination of electrostatic, hydrogen bond, and van der Waals forces, as determined from protein modeling.[13] These materials are formed by around 10 monomers that organize in a single molecular layer as a nanoscale disk.[13b,14] A major driver of the assembling process is the N-terminal domain, namely, the peptide T22. This cationic protein segment is an engineered version of polyphemusin II from Atlantic horseshoe crab *Limulus polyphemus*, which is a well-known antagonist of the cell surface cytokine receptor CXC chemokine receptor type 4 (CXCR4).[15] CXCR4 is used by the human immunodeficiency virus to initiate cell infection,[16] but, in addition, it is an important stem-cell marker in several common human cancers,[17] including metastatic colorectal cancer.[18] T22 specifically and efficiently binds to and penetrates CXCR4$^+$ cells via CXCR4-specific endocytosis, both in vitro and in vivo.[19] T22-mediated uptake of materials is dramatically favored when the ligand is presented in an oligomeric form,[20] probably because of the cooperative multimeric cell binding though simultaneous receptor−ligand interactions.[9a] Therefore, whereas CXCR4 and its specific ligand T22 have proved clinical relevance regarding cell-targeted antitumoral drug delivery,[9b] the structural basis of T22-mediated NP formation is not known. In this context, we have taken here diverse biophysical approaches, mainly spectrofluorimetry and spectropolarimetry, to explore how these T22-empowered polypeptides acquire conformation compatibility with their assembly as CXCR4$^+$ tumor-targeted NPs. For that, T22-GFP-H6, usable as an antitumoral drug carrier,[13a] and its derivative T22-DITOX-H6 have been used as models. T22-DITOX-H6 contains, instead of GFP, the active domain of the potent diphtheria toxin,[21] as the resulting material is a self-assembled, self-delivered NP with intrinsic and cell-targeted antitumoral activity.[22] Devoid of any heterologous carrier, T22-DITOX-H6 NPs fulfill the emerging medical concept of vehicle-free nanoscale drugs.[23]

DOI: 10.1021/acs.biomac.8b00924
Biomacromolecules XXXX, XXX, XXX−XXX

MATERIALS AND METHODS

Protein Production and Purification. T22-GFP-H6 is a modular recombinant protein that contains the potent CXCR4 ligand T22 and that spontaneously self-assembles upon bacteria production and protein purification as green fluorescent NPs.[12,13b,19a] T22-DITOX-H6 is a fully engineered derivative of the previous protein, also showing self-assembling properties, that delivers the unfused functional form of a diphtheria toxin fragment into target cells (Figure 1a), as has recently been described.[22] Both proteins were produced in recombinant *Escherichia coli* Origami B (BL21, OmpT$^-$, Lon$^-$, TrxB$^-$, Gor$^-$, Novagen, Darmstadt, Germany) cultures from the engineered plasmid pET22b. Cells were grown at 37 °C in LB medium supplemented with 100 μg/mL ampicillin, 12.5 μg/mL tetracycline, and 15 μg/mL kanamycin. When the OD_{550} of the cultures reached around 0.5 to 0.7, 0.1 mM IPTG (isopropyl-β-D-thiogalactopyranoside) was added and incubated overnight at 20 °C (for T22-GFP-H6 and T22-DITOX-H6 production). Then, cells were collected by centrifugation for 15 min (5000*g* at 4 °C). Cell disruption was performed in a French press (Thermo FA-078A) at 1200 psi. The lysates were then centrifuged for 45 min (15 000*g* at 4 °C), and the soluble fraction was filtered using a pore diameter of 0.2 μm. Proteins were then purified by their H6 region by immobilized metal affinity chromatography (IMAC) using a HiTrap Chelating HP 1 mL column (GE Healthcare, Piscataway, NJ) with an AKTA purifier FPLC (GE Healthcare). Elution was achieved by elution buffer (20 mM Tris-HCl, pH 8; 500 mM NaCl; 500 mM imidazole), and proteins were then dialyzed against carbonate buffer with salt (166 mM $NaCO_3H$, pH 8; 333 mM NaCl). Protein concentration was obtained by the Bradford's assay. Protein production has been partially performed by the ICTS "NANBIOSIS", more specifically by the Protein Production Platform of CIBER-BBN/IBB (http://www.nanbiosis.es/unit/u1-protein-production-platform-ppp/).

Preparation of Nanoparticles and Unassembled Subunits. Upon purification, the T22-derived protein NPs occur as an unbalanced mixture of NPs and unassembled protomers[14] that are separated by size-exclusion chromatography through a HiLoad Superdex 16/600 200 pg column at 1 mL/min flow rate, as described elsewhere.[14] Such alternative protein versions are, in general, stable in these respective forms,[13a] allowing their further experimental analysis in such forms. This stability is probably due to subtle electrostatic or conformational variability, although assembling and disassembling can be effectively promoted by the manipulation of buffer conditions such as the ionic strength.[24] The starting materials usable for subsequent experiments are described in Figure 1.

Determination of Intrinsic Fluorescence. Fluorescence spectra were recorded in a Cary Eclipse spectrofluorimeter (Agilent Technologies, Mulgrave, Australia). A quartz cell with 10 mm path length and a thermostated holder were used. The excitation and emission slits were set at 5 nm. Excitation wavelength (λ_{ex}) was set at 295 nm. Emission spectra were acquired within a range from 310 to 550 nm. The protein concentration was 0.25 mg/mL in carbonate buffer with salt. To evaluate conformational difference between protomer and NP, we decided to apply the center of spectral mass (CSM) for comparison. CSM is a weighted average of the fluorescence spectrum peak. Also, it is related to the relative exposure of the Trp to the protein environment. The maximum red shift in the CSM of the Trp is compatible with a large solvent accessibility.[25]

The CSM was calculated for each of the fluorescence emission spectra[26] according to eq 1, where I_i is the fluorescence intensity measured at the wavelength λ_i.

$$\lambda = \frac{\sum \lambda_i . I_i}{\sum I_i} \quad (1)$$

Determination of GFP Chromophore Fluorescence. The chromophore fluorescence dependence on the temperature was also evaluated. Fluorescence spectra were recorded in a Cary Eclipse spectrofluorimeter (Agilent Technologies). A quartz cell with 10 mm path length and a thermostated holder were used. The excitation slits set at 2.5 nm and emission slits were set at 5 nm. λ_{ex} was set at 488 nm. Emission spectra were acquired within a range from 500 to 650 nm. T22-GFP-H6 concentration was 0.25 mg/mL in carbonate buffer with salt.

Fluorescence Resonance Energy Transfer within T22-GFP-H6. The unique GFP tryptophan (Trp) is located 1.3 to 1.5 nm away from the chromophore. So, an efficient energy transfer from Trp to the chromophore should be possible. Fluorescence resonance energy transfer (FRET) analysis was developed by exciting the GFP sample at λ_{ex} = 295 nm and reading the fluorescence emission at 513 nm. Emission spectra were acquired within a range of 500 to 650 nm. The protein concentration used was 0.25 mg/mL in carbonate buffer with salt.

Dynamic Light Scattering. The volume size distribution of NPs was determined at 0.25 mg/mL in carbonate buffer with salt by dynamic light scattering (DLS) at 633 nm (Zetasizer Nano ZS, Malvern Instruments Limited, Malvern, U.K.). Samples were maintained at the indicated temperature for 5 min before the measurement. The heating rate for thermal profiles was set at 1 °C/min.

Electron Microscopy (EM). The ultrastructural morphometry (size and shape) of unassembled protomers and NPs was determined at nearly native state both by deposition on silicon wafers with field-emission scanning electron microscopy (FESEM) and by negative staining with transmission electron microscopy (TEM). Drops of 3 μL of NPs and unassembled versions of T22-GFP-H6 and T22-DITOX-H6 at 0.25 mg/mL in carbonate buffer with salt were directly deposited on silicon wafers (Ted Pella, Reading, CA) for 1 min, and the excess of liquid was blotted with Whatman filter paper number 1 (GE Healthcare), air-dried for few minutes, and immediately observed without coating with a FESEM Zeiss Merlin (Zeiss, Oberkochen, Germany) operating at 1 kV equipped with a high-resolution in-lens secondary electron detector. Drops of 3 μL of the same four samples were directly deposited on 200-mesh carbon-coated copper grids (Electron Microscopy Sciences, Hatfield, PA) for 30 s, and the excess was blotted with Whatman filter paper, contrasted with 3 μL of 1% uranyl acetate (Polysciences, Warrington, PA) for 1 min, blotted again, and observed in a TEM JEOL 1400 (Jeol, Tokyo, Japan) operating at 80 kV equipped with a Gatan Orius SC200 CCD camera (Gatan, Abingdon, U.K.). For each sample and technique, representative images of different fields were captured at high magnifications (from 100 000× to 500 000×).

Circular Dichroism. Measurements were made with a JASCO J-715 spectropolarimeter (JASCO, Oklahoma City, OK) with a thermostated device by a Peltier system. spectropolarimeter using a 1 mm path length quartz cell. Each spectrum was an average of six scans. The protein concentration was adjusted to 0.25 mg/mL in carbonate buffer with salt. Scan speed was set at 50 nm/min with a 1 s response time. Molar ellipticity was calculated according to eq 2.

$$[\theta]_{\lambda}^{MRW} = \frac{MRW \times \theta}{l \times c} \quad (2)$$

where MRW is the mean residue molecular weight calculated from the protein sequence, θ is the measured ellipticity (in degrees) at a given wavelength, l is the path length in millimeters, and c is the protein concentration in g/mL. Measurements were carried out in the 200−260 nm region. Molar ellipticity units were deg cm^2 dmol^{-1} residue^{-1}. For the thermal studies, the heating rate was set at 1 °C/min.

RESULTS

T22-GFP-H6 and its derivative T22-DITOX-H6 (Figure 1a) have been produced in recombinant bacteria as single molecular species (Figure 1b) and obtained as either unassembled protomers or assembled NPs (Figure 1b,c), with sizes and molecular architecture described elsewhere.[13b,22] This fact allows the comparative analysis of the conformation acquired by these proteins in each supramolecular form. For that, intrinsic fluorescence spectrum and circular dichroism

DOI: 10.1021/acs.biomac.8b00924
Biomacromolecules XXXX, XXX, XXX−XXX

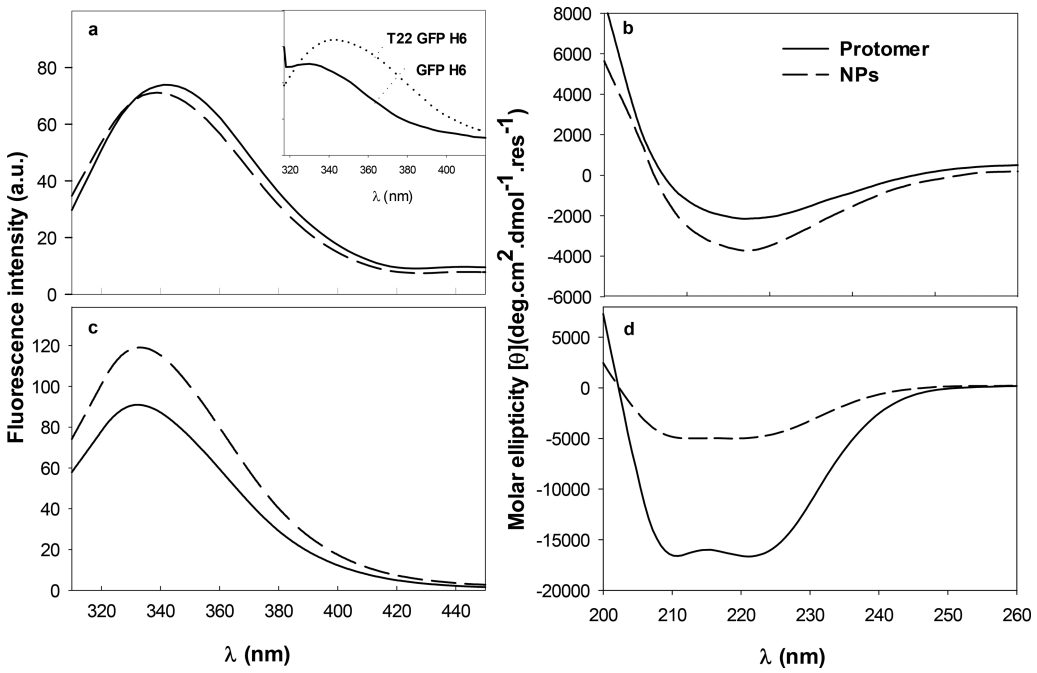

Figure 2. Protein spectroscopy obtained at 25 °C for the protomer (whole line) and the NP (dashed line) versions. (a) T22-GFP-H6 Trp fluorescence spectra. (b) T22-GFP-H6 CD spectra. (c) T22-DITOX-H6 fluorescence spectra. (d) T22-DITOX-H6 CD spectra.

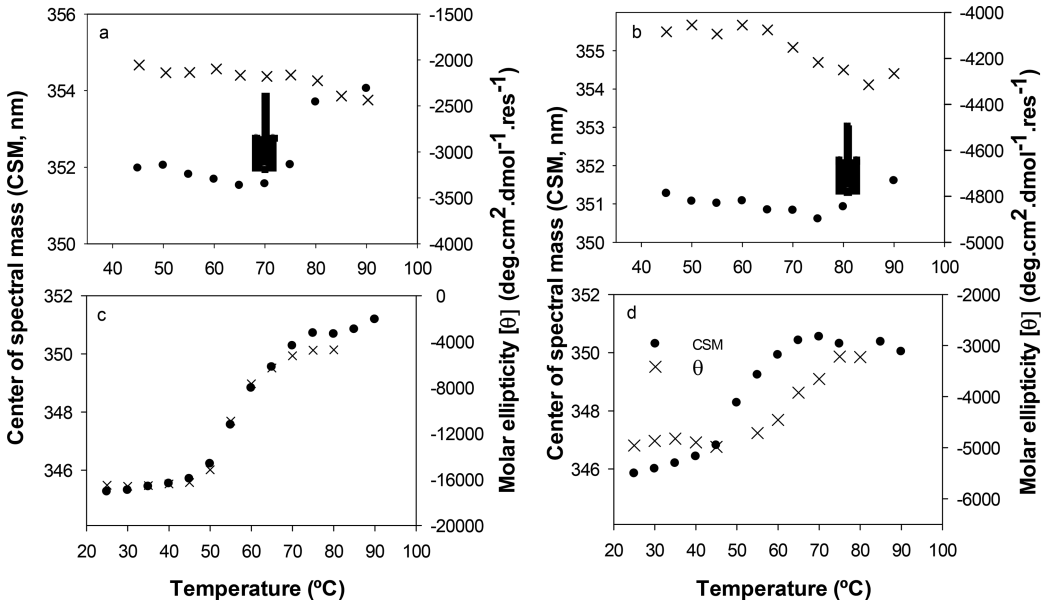

Figure 3. Protein thermal unfolding measured by the center of spectral mass of the Trp fluorescence spectrum CSM (black symbols) and by far-UV CD molar ellipticity values (× symbols) at (a,b) 218 and (c,d) 222 nm. (a,b) T22-GFP-H6 protomer and NPs, respectively. (c,d) T22-DITOX-H6 protomer and NPs, respectively.

spectrum of each protein versions were determined to identify possible structural changes as the monomer undergoes conversion into NPs. In tryptophan (Trp)-containing proteins, the amino acid fluorescence dominates the emission spectrum upon excitation at 295 nm, and it results in being sensitive to the molecular environment.[26] This property is related to the protein globular conformation. Initially, the T22-GFP-H6 Trp fluorescence spectrum was performed (Figure 2a). GFP contains only one Trp located 1.3 to 1.5 nm away from the chromophore, and efficient energy transfer from Trp to the green chromophore should be possible. This fact explains the low-intensity values for Trp fluorescence emission in GFP-H6.[27] Besides, T22 contains only one Trp residue located after two arginines from the amino terminal sequence. Therefore, the higher accessibility to the molecular environment reflected a more hydrated or polar environment for Trp from T22. The inset from Figure 2a proved that in this protein the Trp fluorescence signal comes mainly from the cationic peptide instead of GFP domain. Because T22 seems to be more exposed to the medium,[13b] no visible differences could be detected between both protein formats. However, subtle changes in the fluorescence signal were observed, and T22-GFP-H6 NPs exhibited a discrete displacement of the CSM toward minor values with respect to the protomer. In such NP

DOI: 10.1021/acs.biomac.8b00924
Biomacromolecules XXXX, XXX, XXX−XXX

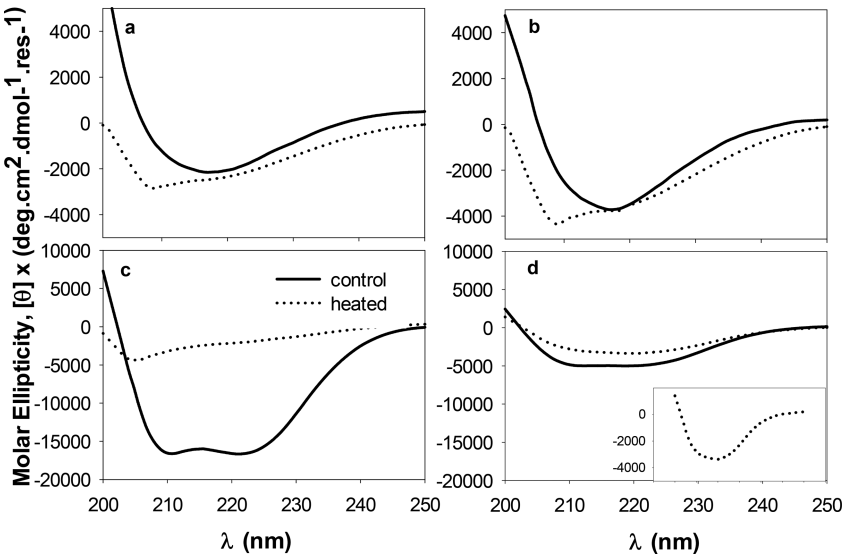

Figure 4. Far-UV CD spectra of T22-GFP-H6 building blocks (a) and NPs (b) and T22-DITOX-H6 building blocks (c) and NPs (d) before (whole line) and after (dashed line) the thermal treatment up to 90 °C for T22-GFP-H6 versions and up to 70 °C for T22-DITOX-H6. The inset details the spectrum of heated T22-DITOX-H6 NPs.

version, new intra- or intermolecular interaction of T22 within the protein assembly appeared (Figure 2a). On the contrary, CD studies demonstrated the highly β--sheet secondary structure of T22-GFP-H6, with a spectrum minimum at 217 nm (Figure 2b, whole line). The oligomeric form of T22-GFP-H6 exhibited an inconspicuous increase in beta structure extent with respect to the protomer (Figure 2b, dashed line). The minimum increase was only 2000 molar ellipticity units (from −2000 to −4000).

On the contrary, T22-DITOX-H6 contains five Trp residues, what makes this construct suitable for intrinsic fluorescence analysis. The fluorescence spectrum analysis of this protein obtained at 25 °C turned out a CSM value of 345.2 nm and a maximal wavelength, λ_{max}, of 330 nm (Figure 2c, whole line). These data were compatible with Trp residues localized in a nonpolar environment. It is interesting to compare this CSM value of 345.2 nm with CMS of 352 nm obtained with the T22-GFP-H6 protomer. As mentioned above, the fluorescence signal of the GFP moiety comes from the Trp highly accessible to a polar environment. Within the NPs, the Trp residues of T22-DITOX-H6 sensed a less hydrophobic environment (CMS = 345.9) while λ_{max} moved from 332 to 334 nm (Figure 2c, dashed line or Figure 3c,d, black points from 25 to 40 °C). Although these last results are not drastically different, a remarkable contrast in the far UV CD signal emerged between T22-DITOX-H6 as a protomer and as a NP (Figure 2d).The protomer exhibited highly alpha structure (two spectrum minima at 211 and 222 nm) as previously reported for the catalytic domain of diphtheria toxin.[28] In the assembled form, the alpha structure content seemed to fade away concomitant with the appearance of beta conformation as the two minima become less noticeable (Figure 2d, dashed line). Besides, the secondary structure content analyzed by JASCO spectra-manager analysis software showed an increase in beta structure of 23% (RMS:25%) as the protomer takes part of NPs. In these cases, the spectra wavelength range was 190 to 260 nm.

The unfolding of each protein version was studied by the analysis of the tertiary (center of spectral mass (CSM)) and the secondary (the molar ellipticity value at the spectrum minimum point) structure as the temperature increased. When proteins unfolded, Trp residues moved to a highly hydrated environment and consequently the CSM value grew (Figure 3). On the contrary, the secondary structure faded away versus temperature and an increase in the molar ellipticity was recorded (Figure 3, × symbols). The unfolding temperature (T_m) is the "×" value that corresponds to the inflection point in the curve (Figure 3). In this context, the heating of unassembled T22-GFP-H6 caused a modest increase in the CSM value at 70 °C (Figure 3a), indicating that the protein transited to a more loosely packed structure. Moreover, in T22-GFP-H6 NPs, this event was negligible (Figure 3b). In both versions of T22-GFP-H6, the molar ellipticity seemed to be unaltered while heating (Figure 3a,b, × symbols). Despite that, no visible secondary structure appeared in the CD spectra of T22-GFP-H6 after heating the protein to 90 °C (Figure 4a,b). This indicated that at 90 °C the secondary structure of both formats of T22-GFP-H6 vanished, but it cannot be demonstrated by the thermal profile of the CD value at 222 nm analyses.

In the thermal unfolding of the T22-DITOX-H6 building block, a typical two-state thermal transition was observed. The unfolding temperature (T_m) is 57 °C (Figure 3c). Because fluorescence studies are related to the tertiary structure and far-UV CD deals with the secondary structure of proteins, the overlaid experimental curves confirmed that T22-DITOX-H6 protomer unfolds as a cooperative unit. In contrast, T22-DITOX-H6, assembled as NPs, revealed a more complex thermal unfolding profile. In contrast with what happens with the subunit, the oligomeric protein first loses its tertiary conformation (Figure 3d), and this event occurs at a lower temperature than in the case of protomers (T_m = 52 °C). However, the secondary structure was preserved at higher temperatures with respect to the protomer (T_m = 64 °C) (Figure 3d). This complex thermal unfolding was previously described for other oligomeric proteins.[29] Besides, the data in Figure 4d demonstrate that after heating to 70 °C T22-DITOX-H6 preserved its secondary structure in NPs (see the inset). The molar ellipticity value exhibited by the protomer jumps around 14 000 units from low to high temperatures

DOI: 10.1021/acs.biomac.8b00924
Biomacromolecules XXXX, XXX, XXX−XXX

(from −18 000 to −4000 ellipticity), while the change in molar ellipticity of NPs during the whole heating range is just 2000 units (from −4800 to −3200). Therefore, we confirm that oligomerization confers secondary structure thermal stability to T22-DITOX-H6, although it is still unclear with the situation of T22-GFP-H6 upon heating. To go further into the analyses of NP integrity, we evaluated the hydrodynamic size of the NPs and the possible disassembly associated with temperature increase.

DLS analyses confirmed the oligomeric nature of the NP samples at 25 °C. T22 GFP-H6 protomer showed a size of 5.6 nm (pdi = 0.342), while the NPs measured 12.3 nm (pdi = 0.452) (Figure 5a,c, whole line). Contrary to what is expected

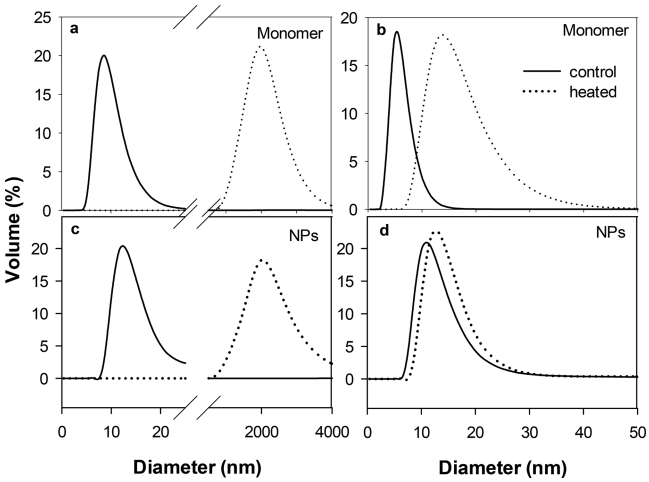

Figure 5. Relative frequency distribution of diameters (volume-weighted distribution) determined by DLS. (a) T22-GFP-H6 protomers, (b) T22-DITOX-H6 protomers, (c) T22-GFP-H6 NPs, and (d) T22-DITOX-H6 NPs. The hole line represents the measurement at 25 °C and the dashed line represents the measurement at 70 (for T22-DITOX-H6) or 85 °C (for T22-GFP-H6).

when the protein was heated to 85 °C, the building block acquired on average an oligomeric size of 13.5 nm (pdi = 0.178), equally from that presented by the heated NPs (13.5 nm (pdi = 0.159)). Therefore, the disassembling of NPs as temperature increased was ruled out. It is noteworthy that, in fact, the heated samples displayed higher particle size, a phenomenon that could be related to the highly hydrated or unfolding nature of T22-GFP-H6. The reason for acquiring a similar particle size would need further investigation, but it could be related to the appearance of an oligomeric transition state during unfolding in the NPs as in the protomer. The unassembled T22-DITOX-H6 exhibited a molecular size of 8.72 nm (pdi = 0.596) at 25 °C (Figure 5b, whole line), and the NP size was on average 12.3 nm (pdi = 0.293) (Figure 5d, whole line). When both samples were heated to 70 °C, the proteins were completely aggregated (Figure 5d, dashed line). These last DLS size measurements of protomers and NPs were ∼1990 nm (pdi = 0.25), far from the detection limit of the equipment. Despite the NP coagulation state, they seemed to retain secondary structure, as demonstrated by data in Figure 3d (dashed line or inset). In addition, data in the inset of Figure 4d also supported the preservation of secondary structure while heating.

Later, we take advantage of the internal FRET phenomenon that occurs within the protein. Interestingly, the fluorescence of the green chromophore excited at 488 nm (λ_{ex}) was practically the same within both versions (Figure 6a). On the

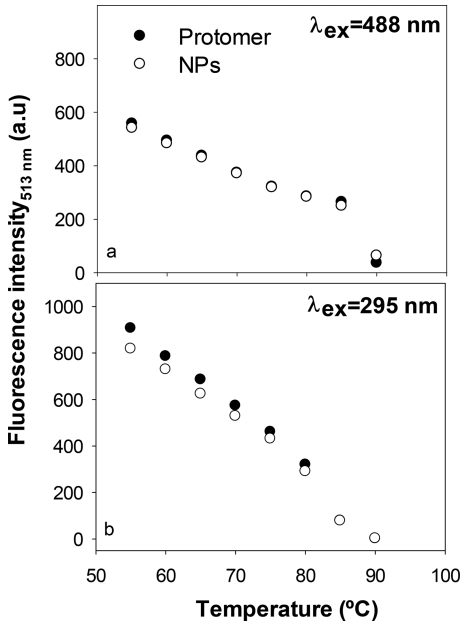

Figure 6. T22-GFP-H6 chromophore fluorescence intensity (at 513 nm) decrease versus temperature measured at two different λ_{ex}/wavelengths (a) λ_{ex} = 488 nm and (b) λ_{ex} = 295 nm.

contrary, we evaluated the internal FRET as described in the Materials and Methods. Surprisingly, the fluorescence decay occurs with different slopes, depending on the supramolecular state of T22-GFP-H6 up to 80 °C (Figure 6b) ($slope_{Protomer}$ = −23 ± 0.5 and $slope_{NPs}$ = −20 ± 0.7). Beyond this temperature, both protein versions exhibited the same fluorescence intensity, suggesting that up to 80 °C there is subtle remoteness between the fluorophores concomitant with distinct structural features within NPs. Above 80 °C, similar protein structure exhibited similar fluorescence values (Figure 6a) and similar sizes (Figure 5 a,c)

In an attempt to assess that the subtle structural qualities of NPs with respect to T22-GFP-H6 protomer modulate the thermal stability up to 80 °C, we studied the thermal reversibility of the internal FRET upon heating. The obtained data demonstrated that upon cooling from 80 °C, the protein within the NPs recovered 62% of the initial fluorescence at 40 °C (Figure 7a,b).

On the contrary, the heating of the protein samples to 90 °C demonstrated that the recovery of fluorescence values after cooling to 40 °C was negligible for both protein versions (Figure 7c,d). Then, we can conclude that a subtle structural difference appears in both T22-GFP-H6 versions that is maintained until the protein sample is heated to 80 °C.

DISCUSSION

Peptide and protein self-assembling is a complex thermodynamic process[30] whose control, even partial, might allow the generation of promising protein-based materials with a spectrum of biomedical applications, especially in drug delivery.[2a,b,4,8,31] Several types of protein NPs for industrial or biomedical applications have been generated by exploiting

DOI: 10.1021/acs.biomac.8b00924
Biomacromolecules XXXX, XXX, XXX−XXX

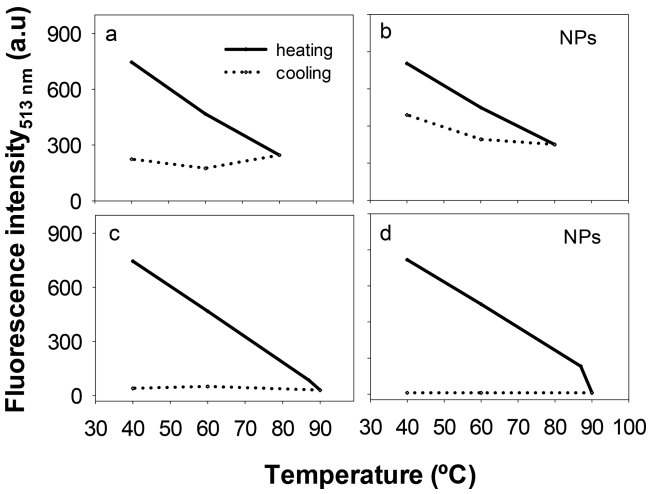

Figure 7. T22-GFP-H6 chromophore fluorescence intensity (at 513 nm, λ_{ex} = 295 nm) as heating−cooling cycle. (a,b) Heating to 80 °C and cooling to 40 °C. (c,d) Heating to 90 °C and cooling to 40 °C.

the hydrophobic interactions between short amylogenic peptides[32] or the structural plasticity of transmembrane proteins,[33] among others. In the context of the emerging interest of artificial viruses as drug delivery agents,[9a,34] antimicrobial peptides[9b,35] and a diversity of proteins and protein segments[1b,2c] have been genetically instructed to self-assemble as mimetics of viral capsids for cell-targeted drug or gene delivery. Such materials are structurally distinguishable from those based on amyloid fibrils,[1a,d,5] which are being developed as well using different nanoscale architectonic principles.

A category of GFP-based oligomeric NPs (T22-GFP-H6) and a potent self-targeted, self-delivered, nanostructured protein drug (T22-DITOX-H6, Figure 1), fully representative of the vehicle-free emerging concept in nanomedicine,[23] have been explored here regarding the conformational changes undergone during oligomerization. These NPs organize as symmetric toroid architectures[13b] whose assembly appears to be initiated by electrostatic cross-molecular contacts[12] and supported by a diversity of noncovalent interactions between building blocks (including hydrogen bond and van der Waals interactions).[13a] The C-terminal histidine-rich domain has a prevalent role in the oligomerization process because imidazole is a potent disruptor of the material once formed.[24] The resulting nanoscale materials are highly soluble, do not form fibrils, and show a moderate content of cross-molecular β-sheet conformation compared with amyloidal aggregates of the same protein species,[13b,36] supportive of a nonamylogenic character. These types of protein-only constructs are supported by a modular multidomain architecture, and they are especially appealing regarding the design of innovative tumor-targeted cancer medicines, where T22-DITOX-H6 is a paradigmatic representative. Produced by biological fabrication in a single step, they self-deliver therapeutic proteins with cytotoxic activities, such as human pro-apoptotic factors, toxins, or venom components, in a nanostructured way and with a high level of selectivity for specific tumor markers.[9b,37] The use of human proteins or deimmunized toxin versions as the main component of these novel drugs, in constructs that do not contain heterologous protein segments (or as minor components), is expected to minimize or eliminate the risk of immune reactions that might be associated with the repeated administration of nonhuman polypeptides as therapeutics.[38]

In general, how proteins adopt their conformation during controlled self-assembling to form nonamyloid materials is a neglected issue but is of pivotal relevance in the context of the growing interest in protein-based functional materials.[2a,b,4,6a,8] In the oligomeric state, the GFP-based T22-GFP-H6 construct presents a shift on λ_{max} values and an increase in the CD signal (Figure 2a,b, respectively). T22-GFP-H6 contains two Trp residues (one within GFP and the other within T22). Their emission (expressed as CSM value) senses a higher hydrophobic environment compared with this phenomenon in the subunit (Figure 2a). Besides, an important proportion of the fluorescence comes from T22 (Figure 2a, inset). These results, concomitant with an increase in the beta structure content in the NP forms (Figure 2b), are in agreement with the concept that the structural conformation is explained by the appearance of the intermolecular interactions in the NPs. Nevertheless, the expansion of the structural information obtained by internal FRET experiments proves that subtle structural rearrangements emerge in GFP moieties of the protein once assembled in NPs. Overall, the described structural features are related to a resilient conformation (Figure 6a,b) of the NPs until 80 °C with respect to their unassembled, individual building blocks. After a thermal heating to 85 °C/90 °C, an unfolded structure is achieved (Figure 4a,b) Surprisingly, both protomers and NPs reached the same oligomer size (Figure 4b,d), suggesting that particular oligomeric forms could also represent an intermediate transition state in the thermal unfolding of the unassembled version.

Finally, DITOX-based NPs present a notably distinct conformation with respect to the subunit version. As NPs, the fusion protein exhibits lesser alpha content and higher beta structure than the protomer version (Figures 2d and 3 d). This result is concomitant with those obtained with fluorescence analyses, like the modest increase in the CSM values in NPs with respect to the subunits (Figure 2c,d) that could be related to the increase in the functionality of DITOX-based NPs. Interestingly, the secondary structure of the NP version remains practically changeless up to 70 °C, and the protein gets aggregated in stable and well-formed NPs (Figures 4d and 5d).

All of these data, apart from the explanation of the conformational transition of protein building blocks into nonamyloid protein NPs, suggest a higher structural stability of the proteins once assembled compared with the unassembled versions. In fact, this NP thermodynamic stability could represent a kinetically trapped state of the proteins, as demonstrated in our previous analyses[12,24] and still under study. Such notably high stability of the oligomers had been already observed in vivo, where a proper tissue targeting and excellent tumor biodistribution are achieved by T22-empowered NPs but not by the equivalent unassembled protein versions.[13a] The data presented here strongly push toward the use of oligomeric versions of cell-targeted drugs or vehicles versus the monomeric or dimeric versions employed in immunotoxins, antibody−drug nanoconjugates, and other innovative drugs.[9b] Structurally, protein-based oligomers might offer all of the conditions for the optimal mimicking of protein-based natural nanoscale agents so that such viruses are ideal regarding tissue penetrability, multivalent ligand presentation, and intracellular cell delivery.[9a,39]

DOI: 10.1021/acs.biomac.8b00924
Biomacromolecules XXXX, XXX, XXX−XXX

CONCLUSIONS

The results presented in this study demonstrate the novel conformation and structure acquired by T22-empowered polypeptides as building blocks of regular homo-oligomers, which is compatible with their functionality as CXCR4$^+$ tumor-targeted NPs. While the internal compactness of the polypeptide is dependent on the specific amino acid sequence located between the cationic and histidine-rich terminal peptides (see the differences between GFP and DITOX), oligomerization occurs concomitantly to an increase in beta structure, which seems to be associated with a thermal stabilization of the protein in the complex. Whether this enhanced structural stability is connected to an improved functional stability, thus supporting the high in vivo performance of these NPs, needs to be further investigated. This structural profiling adds clues for the further design of self-assembling protein NPs that, like T22-DITOX-H6, base both architecture and therapeutic activity on the conformation of the assembled protein.

AUTHOR INFORMATION

Corresponding Authors

*E.V.: E-mail: Esther.vazquez@uab.es.

*A.V.: E-mail: Antoni.villaverde@uab.es.

ORCID

Antonio Villaverde: 0000-0002-2615-4521

Present Address

▽M.P.: Institute for Research in Biomedicine (IRB Barcelona), The Barcelona Institute of Science and Technology, Barcelona 08028, Spain.

Author Contributions

The manuscript was written through contributions of all authors. All authors have given approval to the final version of the manuscript.

Notes

The authors declare the following competing financial interest(s): L.S.-G., N.S., U.U., R.M., E.V., and A.V. have authored a patent on the use of self-assembling, tumor-targeted cytotoxic proteins.

ACKNOWLEDGMENTS

Protein production and DLS have been partially performed by the ICTS "NANBIOSIS", more specifically by the Protein Production Platform of CIBER-BBN/IBB (http://www.nanbiosis.es/unit/u1-protein-production-platform-ppp/) and the Biomaterial Processing and Nanostructuring Unit (http://www.nanbiosis.es/portfolio/u6-biomaterial-processing-and-nanostructuring-unit/). J.M.S. is a Career Investigator from CONICET (Government of Argentina), L.S.-G. was supported by a predoctoral fellowship from AGAUR (2017FI_B100063), N.S. was supported by a predoctoral fellowship from the Government of Navarra, and U.U. received a Sara Borrell postdoctoral fellowship from AGAUR. A.V. received an ICREA ACADEMIA award. This study has been funded by the Agencia Estatal de Investigación (AEI) and Fondo Europeo de Desarrollo Regional (FEDER) (grant BIO2016-76063-R, AEI/FEDER, UE), AGAUR (2017SGR-229), and CIBER-BBN (project VENOM4-CANCER) granted to A.V., ISCIII (PI15/00272 cofounding FEDER) to E.V., and ISCIII (PI15/00378 and PIE15/00028, cofounding FEDER) to R.M.

REFERENCES

(1) (a) Li, D.; Jones, E. M.; Sawaya, M. R.; Furukawa, H.; Luo, F.; Ivanova, M.; Sievers, S. A.; Wang, W. Y.; Yaghi, O. M.; Liu, C.; Eisenberg, D. S. Structure-Based Design of Functional Amyloid Materials. *J. Am. Chem. Soc.* **2014**, *136* (52), 18044−18051. (b) Ferrer-Miralles, N.; Rodriguez-Carmona, E.; Corchero, J. L.; Garcia-Fruitos, E.; Vazquez, E.; Villaverde, A. Engineering protein self-assembling in protein-based nanomedicines for drug delivery and gene therapy. *Crit. Rev. Biotechnol.* **2015**, *35* (2), 209−21. (c) Loo, Y.; Goktas, M.; Tekinay, A. B.; Guler, M. O.; Hauser, C. A.; Mitraki, A. Self-Assembled Proteins and Peptides as Scaffolds for Tissue Regeneration. *Adv. Healthcare Mater.* **2015**, *4* (16), 2557−86. (d) Kumar, V. A.; Wang, B. K.; Kanahara, S. M. Rational design of fiber forming supramolecular structures. *Exp. Biol. Med.* **2016**, *241* (9), 899−908. (e) Yeates, T. O.; Liu, Y.; Laniado, J. The design of symmetric protein nanomaterials comes of age in theory and practice. *Curr. Opin. Struct. Biol.* **2016**, *39*, 134−143.

(2) (a) Sutherland, T. D.; Rapson, T. D.; Huson, M. G.; Church, J. S. Recombinant Structural Proteins and Their Use in Future Materials. *Subcell. Biochem.* **2017**, *82*, 491−526. (b) Kobayashi, N.; Arai, R. Design and construction of self-assembling supramolecular protein complexes using artificial and fusion proteins as nanoscale building blocks. *Curr. Opin. Biotechnol.* **2017**, *46*, 57−65. (c) Corchero, J. L.; Vazquez, E.; Garcia-Fruitos, E.; Ferrer-Miralles, N.; Villaverde, A. Recombinant protein materials for bioengineering and nanomedicine. *Nanomedicine* **2014**, *9* (18), 2817−28.

(3) Sanchez-Garcia, L.; Martin, L.; Mangues, R.; Ferrer-Miralles, N.; Vazquez, E.; Villaverde, A. Recombinant pharmaceuticals from microbial cells: a 2015 update. *Microb. Cell Fact.* **2016**, *15*, 33.

(4) Sutherland, T. D.; Huson, M. G.; Rapson, T. D. Rational design of new materials using recombinant structural proteins: Current state and future challenges. *J. Struct. Biol.* **2018**, *201* (1), 76−83.

(5) Knowles, T. P. J.; Mezzenga, R. Amyloid Fibrils as Building Blocks for Natural and Artificial Functional Materials. *Adv. Mater.* **2016**, *28* (31), 6546−6561.

(6) (a) Wei, G.; Su, Z.; Reynolds, N. P.; Arosio, P.; Hamley, I. W.; Gazit, E.; Mezzenga, R. Self-assembling peptide and protein amyloids: from structure to tailored function in nanotechnology. *Chem. Soc. Rev.* **2017**, *46* (15), 4661−4708. (b) Wendell, D. W.; Patti, J.; Montemagno, C. D. Using biological inspiration to engineer functional nanostructured materials. *Small* **2006**, *2* (11), 1324−9.

(7) Dai, B.; Li, D.; Xi, W.; Luo, F.; Zhang, X.; Zou, M.; Cao, M.; Hu, J.; Wang, W.; Wei, G.; Zhang, Y.; Liu, C. Tunable assembly of amyloid-forming peptides into nanosheets as a retrovirus carrier. *Proc. Natl. Acad. Sci. U. S. A.* **2015**, *112* (10), 2996−3001.

(8) Guttenplan, A. P. M.; Young, L. J.; Matak-Vinkovic, D.; Kaminski, C. F.; Knowles, T. P. J.; Itzhaki, L. S. Nanoscale click-reactive scaffolds from peptide self-assembly. *J. Nanobiotechnol.* **2017**, *15* (1), 70.

(9) (a) Unzueta, U.; Cespedes, M. V.; Vazquez, E.; Ferrer-Miralles, N.; Mangues, R.; Villaverde, A. Towards protein-based viral mimetics for cancer therapies. *Trends Biotechnol.* **2015**, *33* (5), 253−8. (b) Serna, N.; Sanchez-Garcia, L.; Unzueta, U.; Diaz, R.; Vazquez, E.; Mangues, R.; Villaverde, A. Protein-Based Therapeutic Killing for Cancer Therapies. *Trends Biotechnol.* **2018**, *36* (3), 318−335.

(10) (a) Holowka, E. P.; Sun, V. Z.; Kamei, D. T.; Deming, T. J. Polyarginine segments in block copolypeptides drive both vesicular assembly and intracellular delivery. *Nat. Mater.* **2007**, *6* (1), 52−7. (b) Liu, L.; Xu, K.; Wang, H.; Jeremy Tan, P. K.; Fan, W.; Venkatraman, S. S.; Li, L.; Yang, Y. Y. Self-assembled cationic peptide nanoparticles as an efficient antimicrobial agent. *Nat. Nanotechnol.* **2009**, *4* (7), 457−63.

(11) Vazquez, E.; Roldan, M.; Diez-Gil, C.; Unzueta, U.; Domingo-Espin, J.; Cedano, J.; Conchillo, O.; Ratera, I.; Veciana, J.; Daura, X.; Ferrer-Miralles, N.; Villaverde, A. Protein nanodisk assembling and intracellular trafficking powered by an arginine-rich (R9) peptide. *Nanomedicine* **2010**, *5* (2), 259−68.

(12) Unzueta, U.; Ferrer-Miralles, N.; Cedano, J.; Zikung, X.; Pesarrodona, M.; Saccardo, P.; Garcia-Fruitos, E.; Domingo-Espin, J.;

DOI: 10.1021/acs.biomac.8b00924
Biomacromolecules XXXX, XXX, XXX−XXX

Kumar, P.; Gupta, K. C.; Mangues, R.; Villaverde, A.; Vazquez, E. Non-amyloidogenic peptide tags for the regulatable self-assembling of protein-only nanoparticles. *Biomaterials* **2012**, *33* (33), 8714−22.

(13) (a) Cespedes, M. V.; Unzueta, U.; Tatkiewicz, W.; Sanchez-Chardi, A.; Conchillo-Sole, O.; Alamo, P.; Xu, Z.; Casanova, I.; Corchero, J. L.; Pesarrodona, M.; Cedano, J.; Daura, X.; Ratera, I.; Veciana, J.; Ferrer-Miralles, N.; Vazquez, E.; Villaverde, A.; Mangues, R. In vivo architectonic stability of fully de novo designed protein-only nanoparticles. *ACS Nano* **2014**, *8* (5), 4166−76. (b) Rueda, F.; Cespedes, M. V.; Conchillo-Sole, O.; Sanchez-Chardi, A.; Seras-Franzoso, J.; Cubarsi, R.; Gallardo, A.; Pesarrodona, M.; Ferrer-Miralles, N.; Daura, X.; Vazquez, E.; Garcia-Fruitos, E.; Mangues, R.; Unzueta, U.; Villaverde, A. Bottom-Up Instructive Quality Control in the Biofabrication of Smart Protein Materials. *Adv. Mater.* **2015**, *27* (47), 7816−22.

(14) Pesarrodona, M.; Crosas, E.; Cubarsi, R.; Sanchez-Chardi, A.; Saccardo, P.; Unzueta, U.; Rueda, F.; Sanchez-Garcia, L.; Serna, N.; Mangues, R.; Ferrer-Miralles, N.; Vazquez, E.; Villaverde, A. Intrinsic functional and architectonic heterogeneity of tumor-targeted protein nanoparticles. *Nanoscale* **2017**, *9* (19), 6427−35.

(15) Murakami, T.; Maki, W.; Cardones, A. R.; Fang, H.; Tun Kyi, A.; Nestle, F. O.; Hwang, S. T. Expression of CXC chemokine receptor-4 enhances the pulmonary metastatic potential of murine B16 melanoma cells. *Cancer Res.* **2002**, *62* (24), 7328−34.

(16) Wilen, C. B.; Tilton, J. C.; Doms, R. W. Molecular mechanisms of HIV entry. *Adv. Exp. Med. Biol.* **2012**, *726*, 223−42.

(17) (a) Klonisch, T.; Wiechec, E.; Hombach-Klonisch, S.; Ande, S. R.; Wesselborg, S.; Schulze-Osthoff, K.; Los, M. Cancer stem cell markers in common cancers - therapeutic implications. *Trends Mol. Med.* **2008**, *14* (10), 450−60. (b) Sun, X.; Cheng, G.; Hao, M.; Zheng, J.; Zhou, X.; Zhang, J.; Taichman, R. S.; Pienta, K. J.; Wang, J. CXCL12/CXCR4/CXCR7 chemokine axis and cancer progression. *Cancer Metastasis Rev.* **2010**, *29* (4), 709−22.

(18) (a) Kim, J.; Mori, T.; Chen, S. L.; Amersi, F. F.; Martinez, S. R.; Kuo, C.; Turner, R. R.; Ye, X.; Bilchik, A. J.; Morton, D. L.; Hoon, D. S. Chemokine receptor CXCR4 expression in patients with melanoma and colorectal cancer liver metastases and the association with disease outcome. *Ann. Surg.* **2006**, *244* (1), 113−20. (b) Liang, Z.; Yoon, Y.; Votaw, J.; Goodman, M. M.; Williams, L.; Shim, H. Silencing of CXCR4 blocks breast cancer metastasis. *Cancer Res.* **2005**, *65* (3), 967−71.

(19) (a) Unzueta, U.; Cespedes, M. V.; Ferrer-Miralles, N.; Casanova, I.; Cedano, J.; Corchero, J. L.; Domingo-Espin, J.; Villaverde, A.; Mangues, R.; Vazquez, E. Intracellular CXCR4(+) cell targeting with T22-empowered protein-only nanoparticles. *Int. J. Nanomed.* **2012**, *7*, 4533−44. (b) Cespedes, M. V.; Unzueta, U.; Alamo, P.; Gallardo, A.; Sala, R.; Casanova, I.; Pavon, M. A.; Mangues, M. A.; Trias, M.; Lopez-Pousa, A.; Villaverde, A.; Vazquez, E.; Mangues, R. Cancer-specific uptake of a liganded protein nanocarrier targeting aggressive CXCR4+ colorectal cancer models. *Nanomedicine* **2016**, *12* (7), 1987−1996.

(20) Xu, Z.; Unzueta, U.; Roldán, M.; Mangues, R.; Sánchez-Chardi, A.; Ferrer-Miralles, N.; Villaverde, A.; Vázquez, E. Formulating tumor-homing peptides as regular nanoparticles enhances receptor-mediated cell penetrability. *Mater. Lett.* **2015**, *154*, 140−143.

(21) Akbari, B.; Farajnia, S.; Ahdi Khosroshahi, S.; Safari, F.; Yousefi, M.; Dariushnejad, H.; Rahbarnia, L. Immunotoxins in cancer therapy: Review and update. *Int. Rev. Immunol.* **2017**, *36*, 207−219.

(22) Sanchez-Garcia, L.; Serna, N.; Alamo, P.; Sala, R.; Cespedes, M. V.; Roldan, M.; Sanchez-Chardi, A.; Unzueta, U.; Casanova, I.; Mangues, R.; Vazquez, E.; Villaverde, A. Self-assembling toxin-based nanoparticles as self-delivered antitumoral drugs. *J. Controlled Release* **2018**, *274*, 81−92.

(23) Shen, J.; Wolfram, J.; Ferrari, M.; Shen, H. Taking the vehicle out of drug delivery. *Mater. Today* **2017**, *20* (3), 95−97.

(24) Unzueta, U.; Serna, N.; Sanchez-Garcia, L.; Roldan, M.; Sanchez-Chardi, A.; Mangues, R.; Villaverde, A.; Vazquez, E. Engineering multifunctional protein nanoparticles by in vitro disassembling and reassembling of heterologous building blocks. *Nanotechnology* **2017**, *28* (50), 505102.

(25) (a) Li, T. M.; Hook, J. W., 3rd; Drickamer, H. G.; Weber, G. Plurality of pressure-denatured forms in chymotrypsinogen and lysozyme. *Biochemistry* **1976**, *15* (25), 5571−80. (b) Ruan, K.; Weber, G. Hysteresis and conformational drift of pressure-dissociated glyceraldehydephosphate dehydrogenase. *Biochemistry* **1989**, *28* (5), 2144−53. (c) Mohana-Borges, R.; Silva, J. L.; Ruiz-Sanz, J.; de Prat-Gay, G. Folding of a pressure-denatured model protein. *Proc. Natl. Acad. Sci. U. S. A.* **1999**, *96* (14), 7888−93.

(26) Lakowicz, J. R.; Kusba, J.; Wiczk, W.; Gryczynski, I.; Szmacinski, H.; Johnson, M. L. Resolution of the conformational distribution and dynamics of a flexible molecule using frequency-domain fluorometry. *Biophys. Chem.* **1991**, *39* (1), 79−84.

(27) Orm, M.; Cubitt, A. B.; Kallio, K.; Gross, L. A.; Tsien, R. Y.; Remington, S. J. Crystal structure of the Aequorea victoria green fluorescent protein. *Science* **1996**, *273* (5280), 1392−5.

(28) Choe, S.; Bennett, M. J.; Fujii, G.; Curmi, P. M. G.; Kantardjieff, K. A.; Collier, R. J.; Eisenberg, D. The Crystal-Structure of Diphtheria-Toxin. *Nature* **1992**, *357* (6375), 216−222.

(29) Sanchez, J. M.; Nolan, V.; Perillo, M. A. beta-galactosidase at the membrane-water interface: a case of an active enzyme with non-native conformation. *Colloids Surf., B* **2013**, *108*, 1−7.

(30) Wang, J.; Liu, K.; Xing, R.; Yan, X. Peptide self-assembly: thermodynamics and kinetics. *Chem. Soc. Rev.* **2016**, *45* (20), 5589−5604.

(31) (a) Yeates, T. O. Geometric Principles for Designing Highly Symmetric Self-Assembling Protein Nanomaterials. *Annu. Rev. Biophys.* **2017**, *46*, 23−42. (b) de Pinho Favaro, M. T.; Sanchez-Garcia, L.; Sanchez-Chardi, A.; Roldan, M.; Unzueta, U.; Serna, N.; Cano-Garrido, O.; Azzoni, A. R.; Ferrer-Miralles, N.; Villaverde, A.; Vazquez, E. Protein nanoparticles are nontoxic, tuneable cell stressors. *Nanomedicine* **2018**, *13* (3), 255−268.

(32) (a) Zou, Q.; Abbas, M.; Zhao, L.; Li, S.; Shen, G.; Yan, X. Biological Photothermal Nanodots Based on Self-Assembly of Peptide-Porphyrin Conjugates for Antitumor Therapy. *J. Am. Chem. Soc.* **2017**, *139* (5), 1921−1927. (b) Liu, K.; Yuan, C.; Zou, Q.; Xie, Z.; Yan, X. Self-Assembled Zinc/Cystine-Based Chloroplast Mimics Capable of Photoenzymatic Reactions for Sustainable Fuel Synthesis. *Angew. Chem., Int. Ed.* **2017**, *56* (27), 7876−7880.

(33) Tarasov, S. G.; Gaponenko, V.; Howard, O. M.; Chen, Y.; Oppenheim, J. J.; Dyba, M. A.; Subramaniam, S.; Lee, Y.; Michejda, C.; Tarasova, N. I. Structural plasticity of a transmembrane peptide allows self-assembly into biologically active nanoparticles. *Proc. Natl. Acad. Sci. U. S. A.* **2011**, *108* (24), 9798−803.

(34) Noble, J. E.; De Santis, E.; Ravi, J.; Lamarre, B.; Castelletto, V.; Mantell, J.; Ray, S.; Ryadnov, M. G. A De Novo Virus-Like Topology for Synthetic Virions. *J. Am. Chem. Soc.* **2016**, *138* (37), 12202−10.

(35) (a) De Santis, E.; Alkassem, H.; Lamarre, B.; Faruqui, N.; Bella, A.; Noble, J. E.; Micale, N.; Ray, S.; Burns, J. R.; Yon, A. R.; Hoogenboom, B. W.; Ryadnov, M. G. Antimicrobial peptide capsids of de novo design. *Nat. Commun.* **2017**, *8* (1), 2263. (b) Castelletto, V.; de Santis, E.; Alkassem, H.; Lamarre, B.; Noble, J. E.; Ray, S.; Bella, A.; Burns, J. R.; Hoogenboom, B. W.; Ryadnov, M. G. Structurally plastic peptide capsules for synthetic antimicrobial viruses. *Chem. Sci.* **2016**, *7* (3), 1707−1711.

(36) Pesarrodona, M.; Ferrer-Miralles, N.; Unzueta, U.; Gener, P.; Tatkiewicz, W.; Abasolo, I.; Ratera, I.; Veciana, J.; Schwartz, S., Jr.; Villaverde, A.; Vazquez, E. Intracellular targeting of CD44+ cells with self-assembling, protein only nanoparticles. *Int. J. Pharm.* **2014**, *473* (1−2), 286−95.

(37) Diaz, R.; Pallares, V.; Cano-Garrido, O.; Serna, N.; Sanchez-Garcia, L.; Falgas, A.; Pesarrodona, M.; Unzueta, U.; Sanchez-Chardi, A.; Sanchez, J. M.; Casanova, I.; Vazquez, E.; Mangues, R.; Villaverde, A. Selective CXCR4(+) Cancer Cell Targeting and Potent Antineoplastic Effect by a Nanostructured Version of Recombinant Ricin. *Small* **2018**, *14* (26), 1800665.

(38) (a) Frokjaer, S.; Otzen, D. E. Protein drug stability: a formulation challenge. *Nat. Rev. Drug Discovery* **2005**, *4* (4), 298−306.

DOI: 10.1021/acs.biomac.8b00924
Biomacromolecules XXXX, XXX, XXX−XXX

(b) Schellekens, H. Bioequivalence and the immunogenicity of biopharmaceuticals. *Nat. Rev. Drug Discovery* **2002**, *1* (6), 457−62.
(39) Mangues, R.; Vazquez, E.; Villaverde, A. Targeting in Cancer Therapies. *Med. Sci.* **2016**, *4* (1), 6.

DOI: 10.1021/acs.biomac.8b00924
Biomacromolecules XXXX, XXX, XXX−XXX